# Low-dimensional Mott material: transport in ultrathin epitaxial $LaNiO_3$ films

**Junwoo Son[1,a)], Pouya Moetakef[1], James M. LeBeau[1], Daniel Ouellette[2], Leon Balents[2], S. James Allen[2] and Susanne Stemmer[1,b)]**

[1]Materials Department, University of California, Santa Barbara, CA 93106-5050, U.S.A.

[2]Department of Physics, University of California, Santa Barbara, CA 93106-5100, U.S.A.

## Abstract

Electrical resistivity and magnetotransport are explored for thin (3 – 30 nm), epitaxial $LaNiO_3$ films. Films were grown on three different substrates to obtain $LaNiO_3$ films that are coherently strained, with different signs and magnitude of film strain. It is shown that *d*-band transport is inhibited as the layers progress from compression to tension. The Hall coefficient is "hole like". Increasing tensile strain causes the film resistivity to increase, causing strong localization to appear below a critical thickness.

[a)] Electronic mail: json@mrl.ucsb.edu

[b)] Electronic mail: stemmer@mrl.ucsb.edu

Electron transport in two-dimensional systems has been extensively studied in normal metals and semiconductors. Recently, quantum confined films of strongly electron correlated materials have attracted renewed interest. For example, theory predicts dramatic changes in the magnetic and electronic properties for the confined "Mott material" $LaNiO_3$, including the possibility of high-temperature superconductivity [1]. Bulk rare-earth nickelates ($RNiO_3$ with $R$ = rare earth cation), to which $LaNiO_3$ belongs, have been extensively researched because they exhibit a metal-insulator transition (MIT) that is a function of the radius of the rare-earth ion [2]. The transition is believed to be bandwidth-controlled and is associated with an expansion (contraction) of the unit cell, which widens (narrows) the bandwidth [3]. More recent investigations have shown that charge ordering also plays a role in the MIT of the nickelates [4]. Unlike the other nickelates in the series, $LaNiO_3$ remains a paramagnetic metal at all temperatures, albeit a strongly correlated one [5,6]. In this Letter, we show that strong localization can be driven in $LaNiO_3$ films by a combination of strain and reduction in dimensionality.

Epitaxial $LaNiO_3$ films with thicknesses between 2.5 and 30 nm were grown by RF magnetron sputtering. Optimized growth parameters (100 mTorr total pressure, 600 °C substrate temperature) resulted in the smallest film lattice parameter and lowest resistivity. Films were grown on (001) surfaces [7] of cubic $(LaAlO_3)_{0.3}(Sr_2AlTaO_6)_{0.7}$ (LSAT), orthorhombic $DyScO_3$ and rhombohedral $LaAlO_3$. $LaNiO_3$ films ($a$ = 0.384 nm [7]) on LSAT and $DyScO_3$ were under tensile strain and films on $LaAlO_3$ were under compressive strain (Table I). Film thicknesses were determined by cross-section transmission electron microscopy for which samples were prepared by mechanical wedge polishing only, as ion-milling damaged the films. High-angle annular dark-field

(HAADF) imaging was performed using a field emission scanning transmission electron microscope (FEI Titan 80-300) operated at 300 kV. Hall bar structures with Ni/Au contacts were fabricated using photolithography and $LaNiO_3$ etching with hydrochloric acid. Temperature-dependent (magneto-)transport measurements were carried out using a Physical Property Measurement System (PPMS, Quantum Design). To obtain the Hall coefficient $R_H$, the Hall resistance $r_H$ needed to be corrected for the magnetoresistance, i.e., $r_H = \left[V_H(B) - V_H(-B)\right]/2I$, where $V_H(B)$ and $V_H(-B)$ are the Hall voltages at positive and negative magnetic field *B*, respectively, and *I* is the current. The Hall coefficient was obtained from $R_H = \left(\partial r_H / \partial B\right) \cdot t$, where *t* is the film thickness.

All $LaNiO_3$ films were coherently strained up to 30 nm on LSAT and $LaAlO_3$ and up to 10 nm on $DyScO_3$. Fig. 1a shows radial high-resolution x-ray diffraction scans through the 002 symmetric reflections of $LaNiO_3$ films and substrates. Thickness fringes indicate smooth and coherent films. The out-of-plane film lattice parameters reflect the film strain (Table I). Figure 1b shows HAADF images of a 3-nm-thick $LaNiO_3$ film on LSAT, which confirmed the cube-on-cube epitaxial orientation relationship. All films are continuous and smooth.

Figure 2a shows the temperature-dependent resistivity of $LaNiO_3$ films on LSAT as a function of thickness. Thick (10 - 30 nm) films show metallic behavior with a resistivity of ~ 150 μΩcm at room temperature, independent of film thickness. This value is comparable to the lowest reported values [6,8], indicating good oxygen stoichiometry [9]. Below ~ 10 nm, the room temperature resistivity increases. The 4-nm-films show a resistivity minimum at ~ 40 K (see inset in Fig. 2a) below which the resistivity scaled with $\log(T)$ (see inset in Fig. 3). Further decrease in film thickness to

3 nm causes the films to become strongly localized (insulating), showing an increase in resistivity with decreasing temperature over the entire temperature range. For films on $DyScO_3$, which are under a larger tensile strain than those on LSAT, the transition to strong localization occurs at a larger thickness (Fig. 2b). *Independent of substrate*, the critical thickness for strong localization of the tensile-strained films corresponds to a film resistance of ~10 $k\Omega/\square$, the Mott minimum metallic conductivity as calculated from the Ioffe-Regel limit [10], where strong localization should appear. Compressive-strained $LaNiO_3$ films on $LaAlO_3$ show lower resistivities than films on LSAT and $DyScO_3$ and no MIT down to 2.5 nm. However, the thinnest (2.5 nm) film on $LaAlO_3$ also shows a resistivity minimum.

The observed resistivity minima and logarithmic temperature dependence in the intermediate regime can be due to weak localization [11,12] or electron-electron interactions [13]. Figure 3 shows that negative magnetoresistance in a perpendicular field is observed below the resistivity minimum. This is consistent with weak localization; a magnetic field suppresses the coherent interference needed for weak localization [11]. The Hall coefficient of $LaNiO_3$ layers on all substrates was positive, "hole" like, while the Seebeck coefficient was negative, similar to bulk $LaNiO_3$ [6,9]. A Fermi surface with any complexity can give rise to opposite signs [14,15]. Band structure calculations and photoemission spectroscopy show small electron Fermi surfaces with an enhanced effective mass at the $\Gamma$ point and a large hole Fermi surface around the R point [15,16]. Figure 4 shows that $R_H$ for films on LSAT and $LaAlO_3$ exhibits a strong temperature dependence, inconsistent with normal metallic behavior, which indicates temperature-dependent scattering times and/or carrier

concentrations/asymmetry [17]. Because two carrier types with different mobilities are present, $R_H$ cannot be easily converted into carrier concentrations [18,19].

At first glance the transport on the three substrates is similar: (*i*) metallic temperature dependence at room temperature for most thicknesses; (*ii*) emerging weak and then strong localization as the layer resistance approaches the Mott minimum conductivity (*iii*) temperature dependent hole-like $R_H$, and (*iv*) thickness dependent $R_H$, *beyond* the trivial $1/t$. Behind these similarities, a systematic trend toward localization or inhibited transport appears, which we will discuss next.

In the literature, thickness-dependent conductivity of metallic oxide thin films has been attributed to a "dead layer" [20]. We use the high temperature resistivity to explore thickness dependence and the potential role of "dead layers". We use a phenomenological, classical description of the resistivity $\rho$:

$$\rho = \left(\frac{m}{n}\right)\frac{1}{e^2}\left(\frac{1}{\tau_{ph}} + \frac{1}{\tau_{surface}} + \frac{1}{\tau_{impurity}}\right), \tag{1}$$

where *e* the electron charge, and the band structure is captured by the term that contains the carrier mass *m* and density *n*. The scattering rate is the sum of *temperature dependent*, intrinsic, phonon scattering ( $\tau_{ph}$) and *temperature independent* terms, such as surface/interface ( $\tau_{surface}$) and impurity ( $\tau_{impurity}$) scattering. The derivative of Eq. (1) with temperature, at high temperature, is given by:

$$\frac{\partial\rho}{\partial T} = \left(\frac{m}{n}\right)\frac{1}{e^2}\frac{1}{\partial T}\left(\frac{1}{\tau_{ph}}\right) \tag{2}$$

Thus $\partial\rho/\partial T$ is independent of *t*, *if* the electrical thickness is equal to the measured thickness (no dead layer) *and* confinement does not produce changes in the band

structure. For thick films on the same substrate, $\partial\rho/\partial T$ at room temperature is similar (see, i.e., Fig. 2a); thus there is no need to invoke position dependent transport such as a "dead layer". The thick film, low temperature (2 – 80 K), resistivity exhibits quadratic temperature dependence, $\rho = \rho_0 + AT^2$, characteristic of electron-electron interactions [5]. Table I shows the coefficients *A* and $\rho_0$, and the high temperature $\partial\rho/\partial T$ (250 – 300 K). Both *A* and $\partial\rho/\partial T$ are measures of changes in intrinsic transport as the biaxial strain evolves from compression to tension. Increasing $\partial\rho/\partial T$ is consistent with a narrowing of the *d*-band with tensile strain. Changes in *d*-band transport drive the films towards a localization transition. As the transport is inhibited the resistance reaches the 2D Ioffe-Regel limit and strong localization sets in. Furthermore, although we are reluctant to over-interpret the Hall data, biaxial expansion may also reduce the effective number of carriers. The results are in keeping with the strong coupling between the lattice deformation and the electronic structure of the nickelates [3,21,22].

This work was supported by the MURI program of the Army Research Office (grant # W911-NF-09-1-0398, program manager: Dr. Marc Ulrich). We thank Ram Seshadri, Nicola Spaldin, Sungbin Lee and James Rondinelli for discussions and Oliver Bierwagen for help with the measurements. This work made use of the MRL facilities supported by the MRSEC Program of the NSF under award No. DMR 05-20415.

## References


[1] P. Hansmann, X. P. Yang, A. Toschi, G. Khaliullin, O. K. Andersen, and K. Held, Phys. Rev. Lett. **103**, 016401 (2009).

[2] J. B. Torrance, P. Lacorre, A. I. Nazzal, E. J. Ansaldo, and C. Niedermayer, Phys. Rev. B **45**, 8209 (1992).

[3] J. L. Garcia-Munoz, J. Rodriguez–Carvajal, P. Lacorre, and J. B. Torrance, Phys. Rev. B **46**, 4414 (1992).

[4] U. Staub, G. I. Meijer, F. Fauth, R. Allenspach, J. G. Bednorz, J. Karpinski, S. M. Kazakov, L. Paolasini, and F. d'Acapito, Phys. Rev. Lett. **88**, 126402 (2002).

[5] K. Sreedhar, J. M. Honig, M. Darwin, M. Mcelfresh, P. M. Shand, J. Xu, B. C. Crooker, and J. Spalek, Phys. Rev. B **46**, 6382 (1992).

[6] K. P. Rajeev, G. V. Shivashankar, and A. K. Raychaudhuri, Solid State Comm. **79**, 591 (1991).

[7] We use the pseudo-cubic unit cells for denoting the surface orientations and lattice parameters for all non-cubic substrates and the $LaNiO_3$ films.

[8] K. Tsubouchi, I. Ohkubo, H. Kumigashira, Y. Matsumoto, T. Ohnishi, M. Lippmaa, H. Koinuma, and M. Oshima, Appl. Phys. Lett. **92**, 262109 (2008).

[9] N. Gayathri, A. K. Raychaudhuri, X. Q. Xu, J. L. Peng, and R. L. Greene, J. Phys.-Condens. Matter **10**, 1323 (1998).

[10] N. F. Mott, Philos. Mag. **26**, 1015 (1972).

[11] G. Bergmann, Phys. Rep. **107**, 1 (1984).

[12] P. A. Lee and T. V. Ramakrishnan, Rev. Mod. Phys. **57**, 287 (1985).

[13] B. L. Altshuler, A. G. Aronov, and P. A. Lee, Phys. Rev. Lett. **44**, 1288 (1980).

[14] S. Fujita and K. Ito, in: Quantum Theory of Conducting Matter (Springer, New York, 2007), p. 195.

[15] N. Hamada, J. Phys. Chem. Solids **54**, 1157 (1993).

[16] R. Eguchi, A. Chainani, M. Taguchi, M. Matsunami, Y. Ishida, K. Horiba, Y. Senba, H. Ohashi, and S. Shin, Phys. Rev. B **79** (2009).

[17] N. Shirakawa, K. Murata, Y. Nishihara, S. Nishizaki, Y. Maeno, T. Fujita, J. G. Bednorz, F. Lichtenberg, and N. Hamada, J. Phys. Soc. Jap. **64**, 1072 (1995).

[18] S. J. Allen, F. Derosa, C. J. Palmstrom, and A. Zrenner, Phys. Rev. B **43**, 9599 (1991).

[19] If magneto transport can be measured in the regime where $\mu_{e,h}B>1$, where $\mu_{e,h}$ is the respective carrier mobility and $B$ is the applied magnetic field, the Hall effect will be a non-linear function of magnetic field and it may be possible to distinguish different carrier contributions, see ref. 18. The layers explored here exhibit linear Hall effect and appear to be far from this limit.

[20] J. Z. Sun, D. W. Abraham, R. A. Rao, and C. B. Eom, Appl. Phys. Lett. **74**, 3017 (1999).

[21] P. Ruello, S. Zhang, P. Laffez, B. Perrin, and V. Gusev, Phys. Rev. B **79**, 094303 (2009).

[22] M. Medarde, P. Lacorre, K. Conder, F. Fauth, and A. Furrer, Phys. Rev. Lett. **80**, 2397 (1998).

Table I: Substrate parameters and $LaNiO_3$ film properties on different substrates for 10 nm thick films.

| Substrate | Lattice parameter (nm) | Lattice mismatch with $LaNiO_3$ (%) | Measured out-of-plane film lattice parameter (nm) | $\frac{\partial\rho}{\partial T}\Big\vert_{250-300K}$ ($\Omega cmK^{-1}$) | $\rho_0\big\vert_{2-80K}$ ($\mu\Omega cm$) | $A\big\vert_{2-80K}$ ($\mu\Omega cmK^{-2}$) |
|---|---|---|---|---|---|---|
| $LaAlO_3$ | 0.375 | -1.32 | 0.3854 | $4.8\times10^{-7}$ | 46 | $1.9\times10^{-3}$ |
| LSAT | 0.387 | 0.78 | 0.3818 | $5.5\times10^{-7}$ | 60 | $2.2\times10^{-3}$ |
| $DyScO_3$ | 0.394 | 2.54 | 0.3779 | $1.3\times10^{-6}$ | 298 | $6.5\times10^{-3}$ |

## Figure Captions

**Figure 1 (color online)**

(a) High-resolution x-ray diffraction radial scans through the 002 reflections of $LaNiO_3$ films and LSAT, $DyScO_3$ and $LaAlO_3$ substrates, respectively. The film thickness were ~ 30 nm on LSAT and $LaAlO_3$ and 10 nm on $DyScO_3$. (b) Low-magnification and (c) atomic resolution cross-section HAADF images of a 3 nm thick $LaNiO_3$ film on LSAT, showing a continuous film.

**Figure 2 (color online)**

Temperature-dependence of the resistivity as a function of $LaNiO_3$ film thickness on (a) LSAT and (b) $DyScO_3$ and (c) $LaAlO_3$. The inset in (a) shows the data for the 4 nm film on a different scale to more clearly show the resistivity minimum at 40 K. The arrows show the resistivity minima for the weakly localized films on all three substrates, i.e. the 4 nm film on LSAT, the 5 nm film on $DyScO_3$ and the 2.5 nm film on $LaAlO_3$. Below these thicknesses, films are strongly localized on LSAT and $DyScO_3$.

**Figure 3 (color online)**

Normalized (to the zero-field value) resistance of the 4 nm $LaNiO_3$ film on LSAT as a function of applied magnetic field and temperature. The inset shows a logarithmic fit to the zero-field resistivity data as a function of temperature.

**Figure 4 (color online)**

$LaNiO_3$ film Hall coefficient as a function of temperature and thickness on LSAT substrates (filled symbols) and $LaAlO_3$ (open symbols).

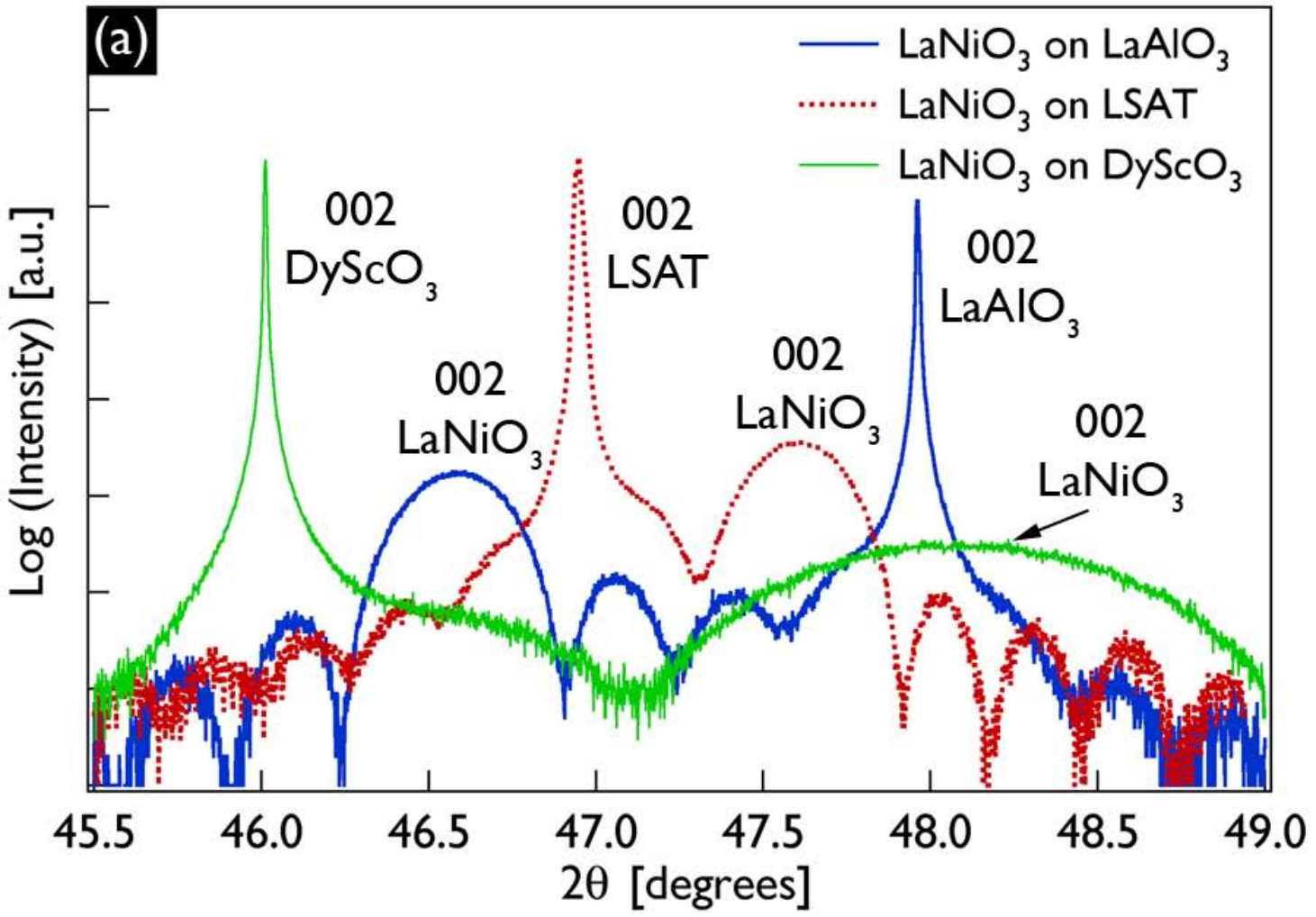
(a)
LaNiO3 on LaAlO3
LaNiO3 on LSAT
LaNiO3 on DyScO3
002 DyScO3
002 LaNiO3
002 LSAT
002 LaNiO3
002 LaAlO3
002 LaNiO3
Log (Intensity) [a.u.]
45.5
46.0
46.5
47.0
47.5
48.0
48.5
49.0
2θ [degrees]

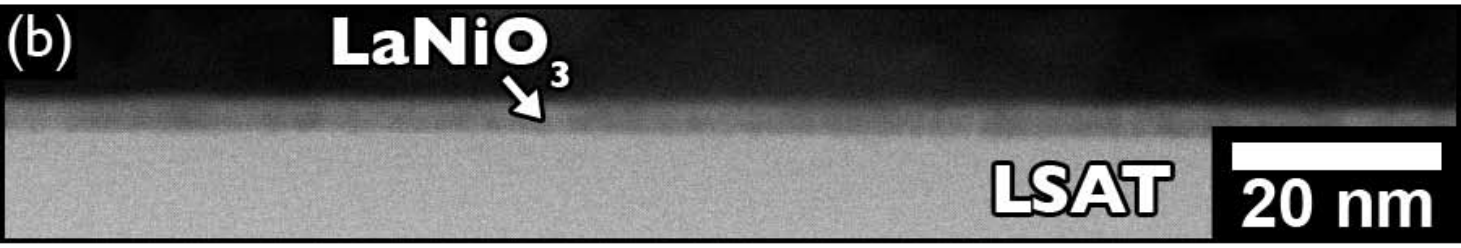
(b)
LaNiO3
LSAT
20 nm

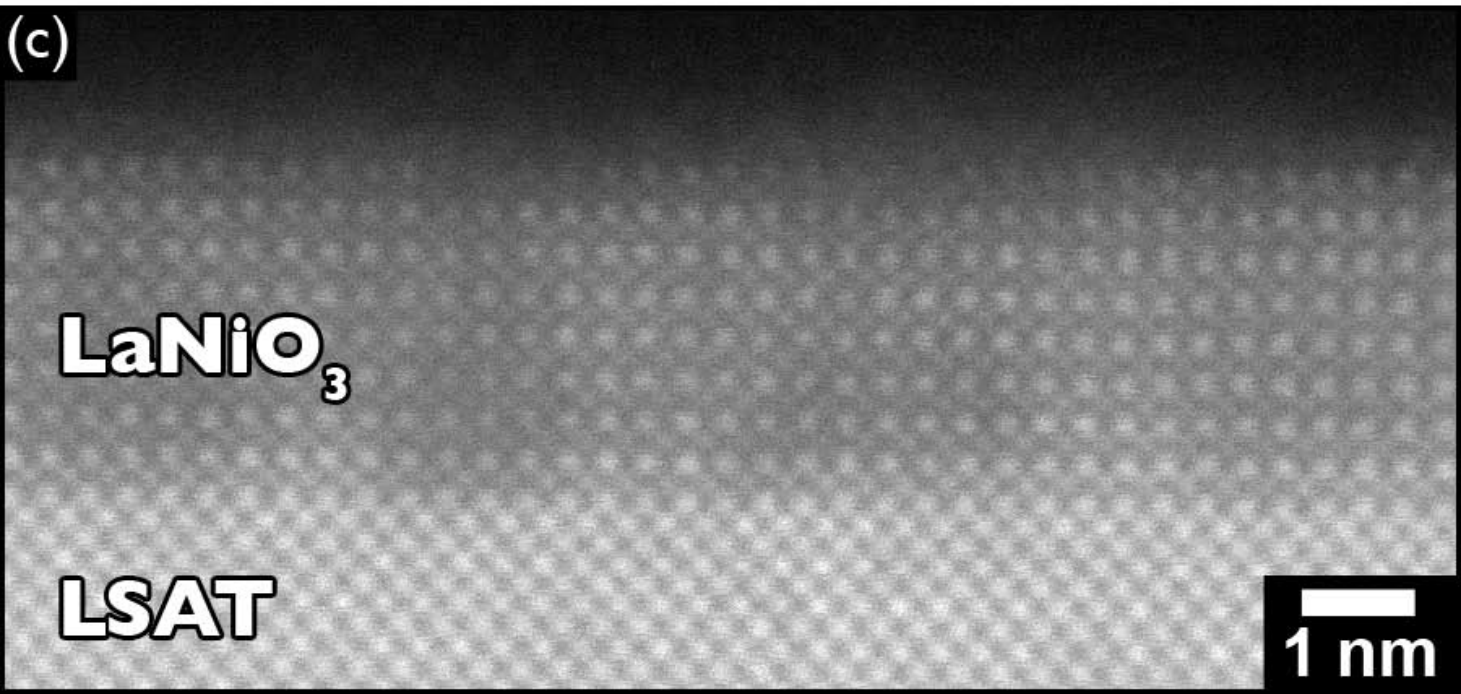
(c)
LaNiO3
LSAT
1 nm

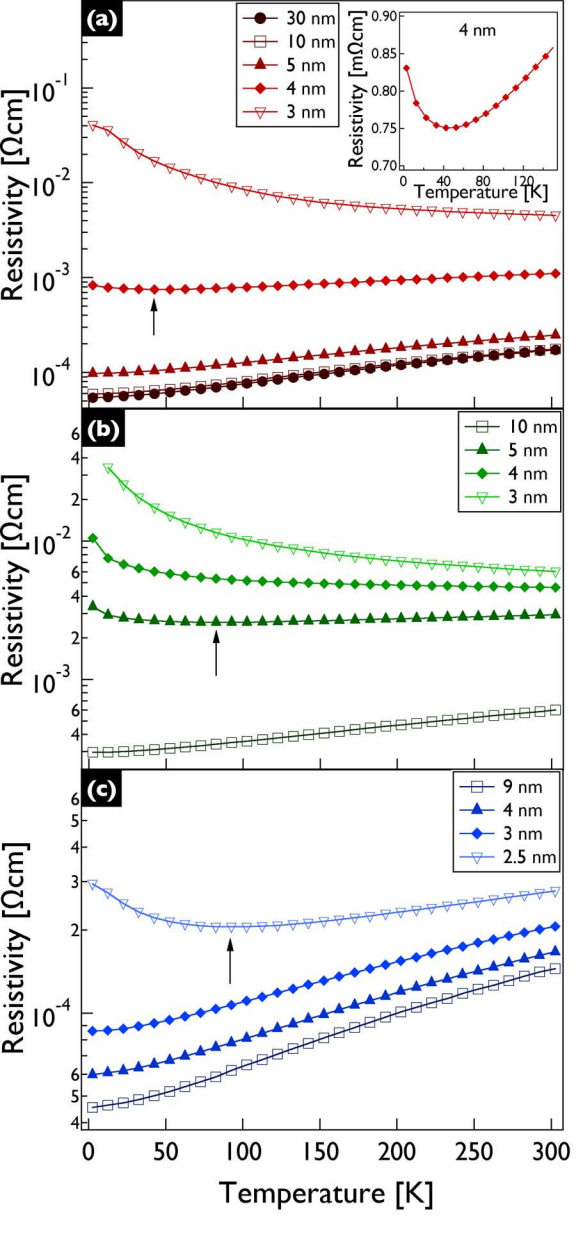
(a)
30 nm
10 nm
5 nm
4 nm
3 nm
4 nm
Resistivity [mΩcm]
Temperature [K]
Resistivity [Ωcm]
(b)
10 nm
5 nm
4 nm
3 nm
Resistivity [Ωcm]
(c)
9 nm
4 nm
3 nm
2.5 nm
Resistivity [Ωcm]
Temperature [K]

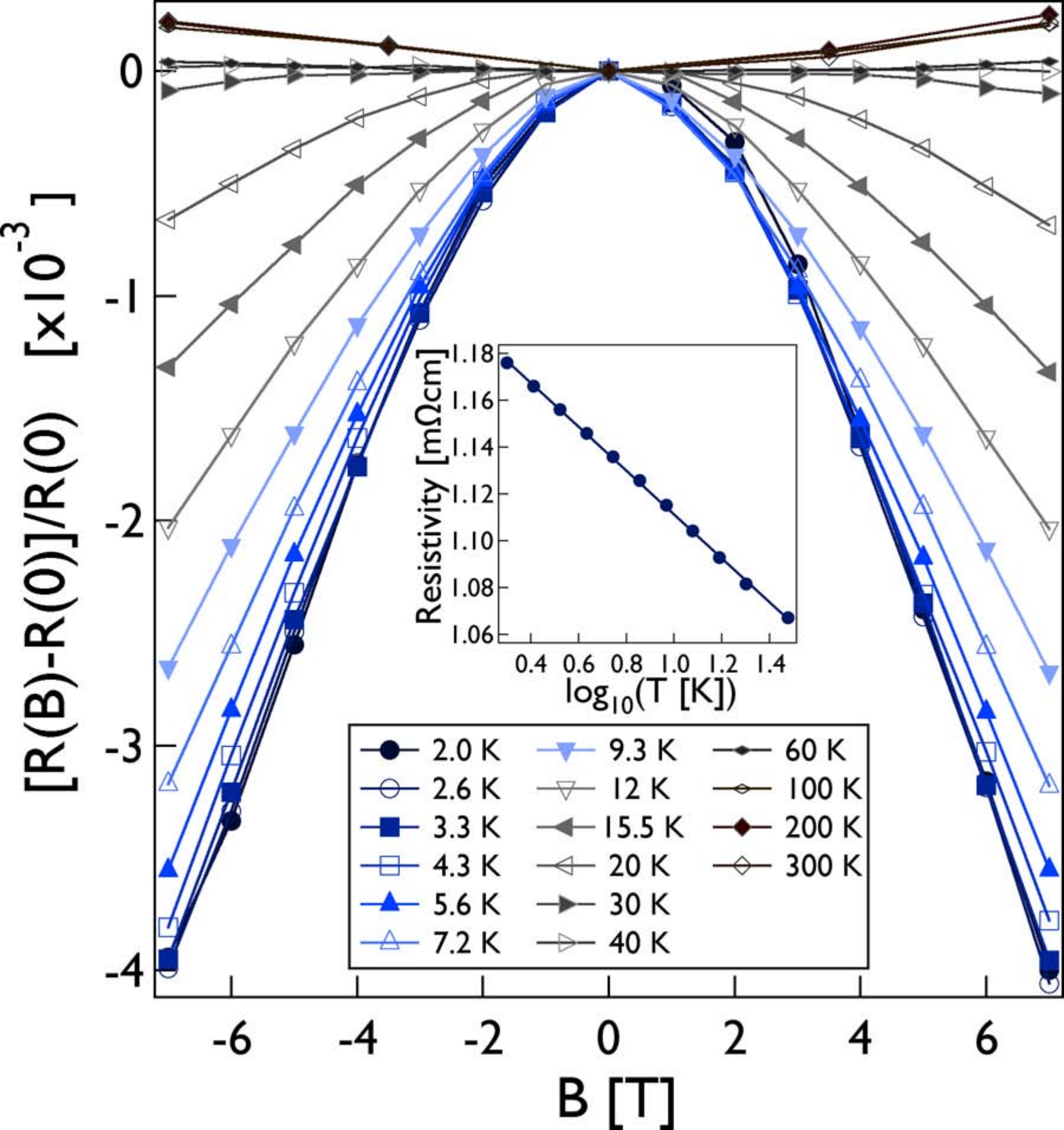
[R(B)-R(0)]/R(0) [x10^-3]
0
-1
-2
-3
-4
-6
-4
-2
0
2
4
6
B [T]
Resistivity [mΩcm]
1.18
1.16
1.14
1.12
1.10
1.08
1.06
0.4
0.6
0.8
1.0
1.2
1.4
log10(T [K])
2.0 K
2.6 K
3.3 K
4.3 K
5.6 K
7.2 K
9.3 K
12 K
15.5 K
20 K
30 K
40 K
60 K
100 K
200 K
300 K

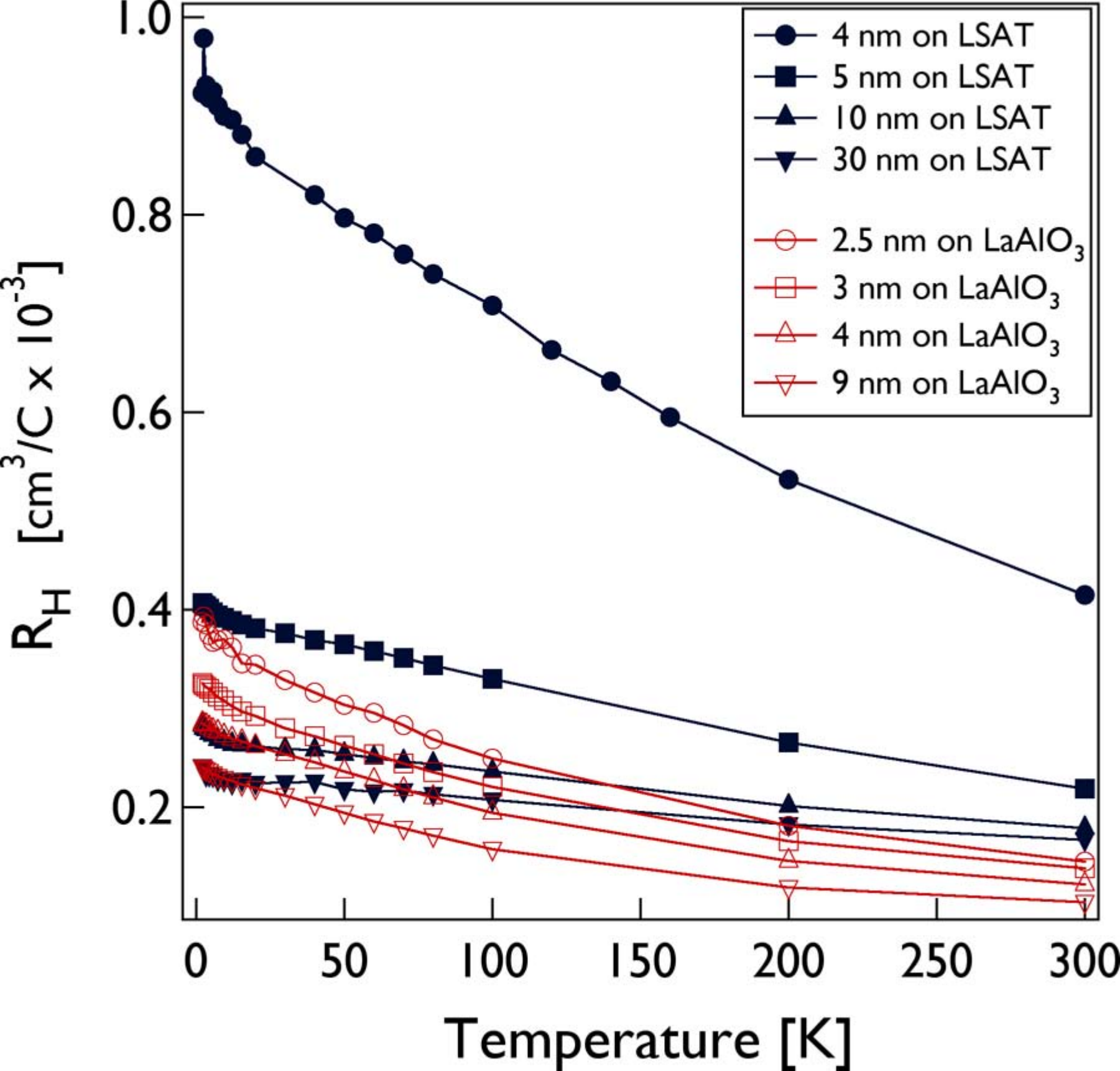
4 nm on LSAT
5 nm on LSAT
10 nm on LSAT
30 nm on LSAT
2.5 nm on LaAlO3
3 nm on LaAlO3
4 nm on LaAlO3
9 nm on LaAlO3
1.0
0.8
0.6
0.4
0.2
R_H [cm^3/C x 10^-3]
0
50
100
150
200
250
300
Temperature [K]